An experimental and theoretical investigation into the design of an active suspension system for a racing car

D J Purdy and **D N Bulman**
Royal Military College of Science, Cranfield University

Abstract: The well-established quarter car representation is used to investigate the design of an active suspension system for a racing car. The work presented is from both a practical and theoretical study. The experimental open-loop and passive responses of the suspension system are used to validate the model and estimate the level of damping within the system. A cascade control structure is used, consisting of an inner body acceleration loop and an outer ride height loop. Comparisons are made between the experimental results and those predicted by the theory.

During the 1980s and early 1990s a number of Formula 1 teams developed active suspension systems to improve the performance of cars. Little detail was published about these systems because of the highly competitive nature of the application. Some of these systems were very sophisticated and successful. Because of this, speed increased considerably and because of the costs involved, the difference in performance between the lower and higher funded teams became unacceptable. For this reason, the governing body of motor sport decided to ban active suspensions from the end of the 1993 racing season. Both authors of this paper were involved with different racing teams at that time, and this paper is an introduction to the very basic philosophy behind a typical active system that was employed on a Formula 1 car.

Keywords: active suspension, modelling, simulation, design, testing

NOTATION

a	area (m^2)
A B C D	state space matrices (system, input, output and transmission respectively)
d	diameter (m)
j	$\sqrt{-1}$
k	stiffness (N/m)
K	controller gain
m	mass (kg)
P	pressure (N/m^2)
q_i	flow rate input to the active suspension actuator (m^3/s)
R	damper valve flow restriction coefficient ($N\,s/m^5$)
$\boldsymbol{u}\ \boldsymbol{x}\ \boldsymbol{y}$	state space vectors (input, state and output respectively)
x	coordinate (m)
η	coordinate for mechanical spring piston (m)

Subscripts

1	actuator volume 1 (see Fig. 1)
2	actuator volume 2 (see Fig. 1)
d	relating to the mechanical spring
p	suspension strut piston
s	body or sprung mass
t	tyre
u	unsprung mass
z	ground input

The MS was received on 4 September 1995 and was accepted for publication on 25 June 1996.

1 INTRODUCTION

The design of a suspension system for a racing car must maintain the ride height and attitude of the vehicle within set limits, so that the aerodynamic (down) force acting on the vehicle remains relatively constant for a given velocity. In this paper the ride height refers to the relative displacement between the body and unsprung mass, though it should be noted that for a Formula 1 car the tyre deflection can have a significant effect on the height of the body from the ground. It is possible for the aerodynamic force to be over twice the static weight of the vehicle and this is

further complicated by the forces generated during braking, accelerating and cornering. To accommodate these large changes in force acting on the car, it is necessary to have high body natural frequencies, in some cases over 5 Hz. One method of overcoming this problem is to use an active suspension system which is capable of maintaining the ride height and attitude of the vehicle at their optimum conditions, while reducing the natural frequencies of the body.

The suspension system of a racing car is set up for each race, thus a control law for the active suspension system must be simple and the effect of changing the gains easily understandable. This requirement eliminates many of the modern control techniques (**1**–**3**) on the grounds of complexity, the controller possibly having to be redesigned for each vehicle set-up. It is also difficult to relate the pole positions or open-loop frequency response to suspension performance.

Many of the classical control laws proposed in the literature (**4**–**8**) make use of measurements of body acceleration and ride height because of the ease with which these parameters can be measured. One commonly used control law (**4**–**7**) uses ride height and absolute body velocity, which is obtained by integrating the body acceleration. One of the reasons for using body velocity is to achieve sky-hook damping, but it should be appreciated that body acceleration feedback with a hydraulic actuator will achieve the same aim. This is the case with this particular study.

Two types of actuator are normally used for an active suspension system (**8**). The first is a double acting ram either alone or in parallel with passive suspension components. The second is a single acting ram acting in series with passive suspension components. With the second configuration it is common for the passive suspension elements, compliance and damping to be incorporated into the actuator. The first type of system requires a greater bandwidth from the controller because it has to control all of the body and unsprung mass modes. For the second type of system, the higher frequency modes associated with the unsprung mass are controlled by the passive suspension characteristics, while the low-frequency modes and ride height are controlled by the actuator and suspension controller. This requires a lower bandwidth from the controller. The second of these types of suspension actuator was used on a Formula 1 system which was familiar to the authors, and has therefore been selected for investigation in this paper.

All modelling of the suspension system and controller design has been performed using linear theory. The paper describes a simple theoretical representation of the system, experimental work on a quarter car rig and a comparison of the results.

2 DESCRIPTION OF THE ACTIVE SUSPENSION SYSTEM

The main component of the active suspension system under consideration was an actuator, originally designed and developed for a Formula 1 application. This is shown diagrammatically in Fig. 1. The actuator consisted of three major elements; a piston, disc type damping valve and a mechanical spring. The piston used low-friction polytetrafluoroethylene (PTFE) guides and seals to reduce the effects of non-linear friction. The damper valve controlled the level of passive damping within the suspension system. This was achieved by directing the oil through different flow paths in bump and rebound using two sets of shims. For the case under investigation, the two sets of shims were identical. Compliance was incorporated into the actuator via a piston and mechanical spring. A mechanical spring was preferred in this application to a possible gas spring (**8**) because of the effect of temperature change. Hydraulic fluid was fed into the actuator from a single servovalve between the damper valve and mechanical spring. An additional port was provided to allow the actuator to be bled during setting up. A displacement transducer was incorporated into the actuator to measure the relative displacement between the body and unsprung mass (ride height). The actuator was located in the suspension system, between the body and unsprung mass, by rod ends at its top and bottom. An on/off valve, included between the servovalve and the actuator, allowed the suspension system to be operated in both passive and active modes.

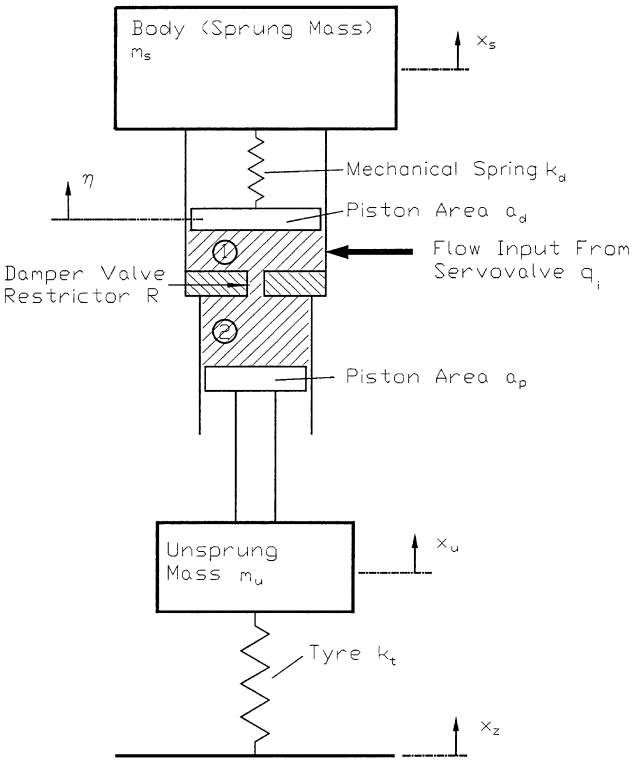

Fig. 1 Mathematical model of the quarter car suspension model

3 THEORETICAL QUARTER CAR SUSPENSION MODEL

The quarter car suspension model is shown in Fig. 1. The equations of motion for the system have been derived under the following assumptions:

(a) the hydraulic fluid is incompressible;
(b) the flow through the damper valve is proportional to the pressure difference across it;
(c) the mechanical spring has been linearized about its nominal operating point;
(d) seals and guides are frictionless;
(e) all coordinates and parameters are measured from their static positions;
(f) no leakage occurs from the system.

The equations for the system have been developed for the following inputs; flowrate from the servovalve (q_i) and ground profile displacement (x_z). The system outputs are ride height ($x_s - x_u$), body acceleration ($\ddot{x}_s$) and unsprung mass acceleration ($\ddot{x}_u$).

Applying Newton's laws of motion to the body and unsprung masses gives

$$m_s\ddot{x}_s = P_2 a_p \tag{1}$$

$$m_u\ddot{x}_u = k_t(x_z - x_u) - P_2 a_p \tag{2}$$

where m_s and m_u are the body and unsprung masses, a_a is the piston area, P_2 is the pressure acting on the piston area and k_t is the tyre stiffness.

Flow continuity in volume 1 gives

$$q_i = \dot{\eta} a_d + (P_1 - P_2)/R \tag{3}$$

where P_1 is the pressure acting on the mechanical spring piston area a_s, η is the coordinate for the mechanical spring piston and R is the damper valve flow restriction coefficient.

The change in pressure in volume 1 is given by

$$P_1 = \frac{\eta k_d}{a_d} \tag{4}$$

where k_d is the stiffness of the mechanical spring.

Flow continuity in volume 2 gives

$$(P_1 - P_2)/R = (\dot{x}_s - \dot{x}_u)a_p \tag{5}$$

By manipulating equations (1) to (5) the mathematical model of the active suspension system can be written in state space form as

$$\begin{aligned} \dot{\boldsymbol{x}} &= \mathbf{A}\boldsymbol{x} + \mathbf{B}\boldsymbol{u} \\ \boldsymbol{y} &= \mathbf{C}\boldsymbol{x} + \mathbf{D}\boldsymbol{u} \end{aligned} \tag{6}$$

where

$$\boldsymbol{x}^T = [x_s \quad \dot{x}_s \quad x_u \quad \dot{x}_u \quad P_1] \tag{6a}$$

$$\boldsymbol{u} = \begin{bmatrix} q_i \\ x_z \end{bmatrix} \tag{6b}$$

$$\boldsymbol{y} = \begin{bmatrix} x_s - x_u \\ \ddot{x}_s \\ \ddot{x}_u \end{bmatrix} \tag{6c}$$

$$\mathbf{A} = \begin{bmatrix} 0 & 1 & 0 & 0 & 0 \\ 0 & \dfrac{-Ra_p^2}{m_s} & 0 & \dfrac{Ra_p^2}{m_s} & \dfrac{a_p}{m_s} \\ 0 & 0 & 0 & 1 & 0 \\ 0 & \dfrac{Ra_p^2}{m_u} & \dfrac{-k_t}{m_u} & \dfrac{-Ra_p^2}{m_u} & \dfrac{-a_p}{m_u} \\ 0 & \dfrac{-k_d a_p}{a_d} & 0 & \dfrac{k_d a_p}{a_d^2} & 0 \end{bmatrix} \tag{6d}$$

$$\mathbf{B} = \begin{bmatrix} 0 & 0 \\ 0 & 0 \\ 0 & 0 \\ 0 & \dfrac{k_t}{m_u} \\ \dfrac{k_d}{a_d^2} & 0 \end{bmatrix} \tag{6e}$$

$$\mathbf{C} = \begin{bmatrix} 1 & 0 & -1 & 0 & 0 \\ 0 & \dfrac{-Ra_p^2}{m_s} & 0 & \dfrac{Ra_p^2}{m_s} & \dfrac{a_p}{m_s} \\ 0 & \dfrac{Ra_p^2}{m_u} & \dfrac{-k_t}{m_u} & \dfrac{-Ra_p^2}{m_u} & \dfrac{-a_p}{m_u} \end{bmatrix} \tag{6f}$$

$$\mathbf{D} = \begin{bmatrix} 0 & 0 \\ 0 & 0 \\ 0 & \dfrac{k_t}{m_u} \end{bmatrix} \tag{6g}$$

The servovalve was modelled with a second-order transfer function, which for a 40 per cent input signal and a supply pressure of 120 bar gives a natural frequency of 90 Hz and a damping ratio of 0.7 (**9**). The data for the suspension system are given in Table 1.

Table 1 Suspension system parameter values and transducer calibration factors

Suspension model parameter	Value
m_s	180 kg
m_u	23 kg
k_d	300 kN/m
k_t	233 kN/m
d_d	0.030 m
d_p	0.028 m
Accelerometers	0.102 V/(m/s^2)
Displacement transducer	180.5 V/m
Servovalve flow coefficient	4.7×10^{-5} m^3/s

4 EXPERIMENTAL MEASUREMENTS

A photograph of the experimental quarter car rig is shown in Fig. 2. The experiments consisted of passive, open-loop and closed-loop testing. The purpose of the passive and open-loop testing was to validate the model and to select a suitable coefficient for the damper valve restrictor. This is described first.

All of the testing was performed using a Solatron 1250 transfer function analyser between 1 and 30 Hz in 149 steps. It may be noted that on the figures, the solid line represents the experimental results.

4.1 Passive testing

The passive responses were obtained by closing the valve between the actuator and the servovalve. The input to the suspension was via a hydraulic actuator under displacement control, see Fig. 2. The measured outputs were the body acceleration, unsprung mass acceleration and the ride height. For comparison with the measured outputs, an accelerometer was used on the ground input.

The responses for the body and unsprung mass acceleration for variations in ground input amplitude are shown in Fig. 3a and b, and for the ride height in Fig. 3c.

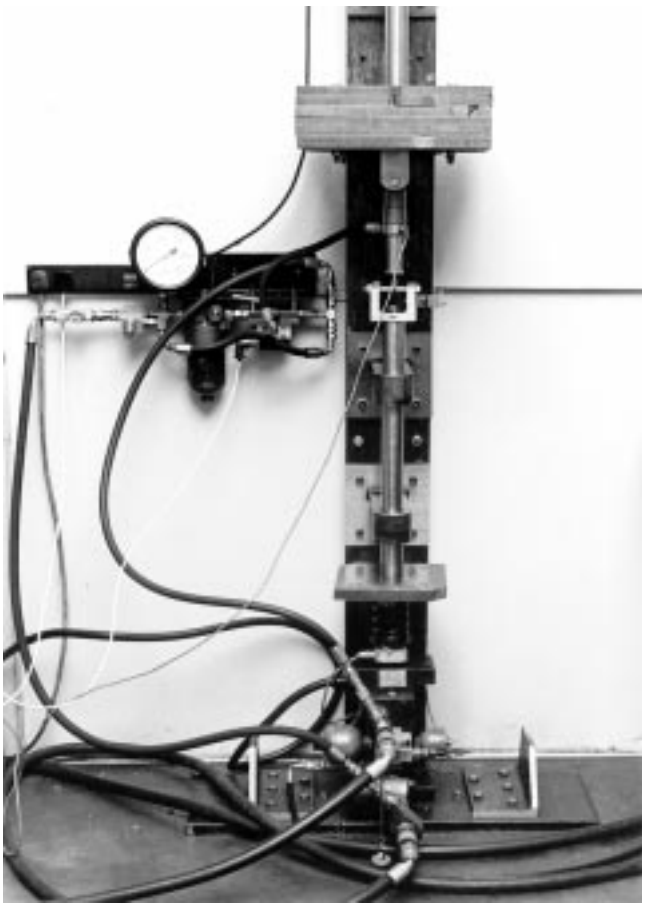

Fig. 2 Active suspension test facility

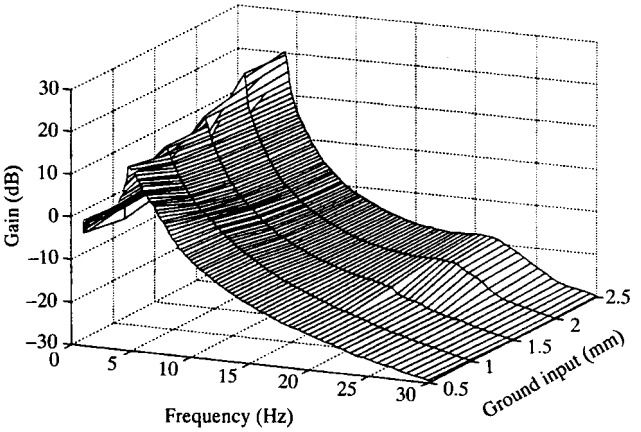

Fig. 3a Passive frequency response (body acceleration/ground acceleration), three-dimensional frequency and ground amplitude versus gain

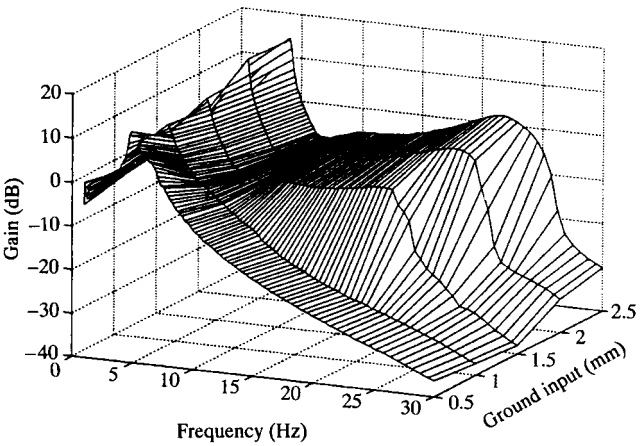

Fig. 3b Passive frequency response (unsprung mass acceleration/ground acceleration), three dimensional frequency and ground amplitude versus gain

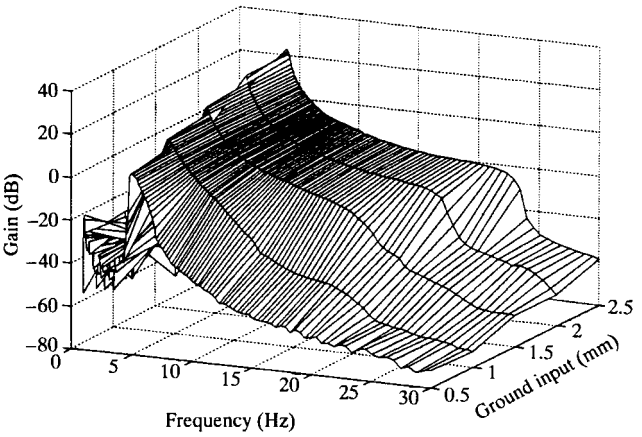

Fig. 3c Passive frequency response (ride height/ground acceleration), three-dimensional frequency and ground amplitude versus gain

At low-amplitude inputs, the non-linear friction causes the actuator to lock out, thus reducing the peak amplitude at the resonances. For a ground input of 2.5 mm the responses for the body, unsprung mass acceleration and ride height are shown in Fig. 4. All these responses show resonances at 4 Hz (the bounce frequency) and 20 Hz (the wheel hop frequency). A weak anti-resonance (zero) for the unsprung mass occurs between 6 and 7 Hz. This is possibly masked by the non-linear friction or level of passive damping, see the Appendix. This anti-resonance is caused by the body on the effective actuator stiffness: this natural frequency is given by $\sqrt{(a_p^2 k_d / a_d^2 m_s)} = 35.6$ rad/s or 5.7 Hz.

4.2 Open-loop testing

The open-loop testing was performed by applying an input voltage to the servovalve current amplifier and monitoring the response of the ride height, body acceleration and unsprung mass acceleration.

It is well known that during this form of test, actuator drift has to be compensated for. However, compensating for actuator drift by simple continuous feedback regulators can affect the validity of the results (**10**). This was overcome by implementing a proportional controller around the strut extension with a constant gain. At each second, the error

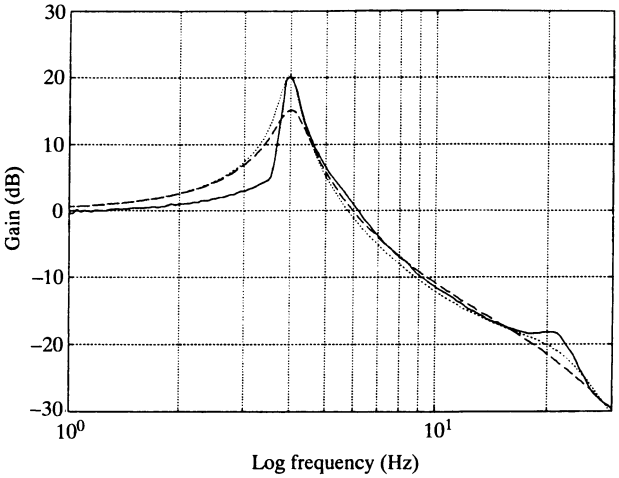

Fig. 4a Passive frequency response gain (body acceleration/ground acceleration), experimental 2.5 mm input (solid line), theoretical $R = 1 \times 10^{10}$ (dashed line) and theoretical $R = 0.5 \times 10^{10}$ (dotted line)

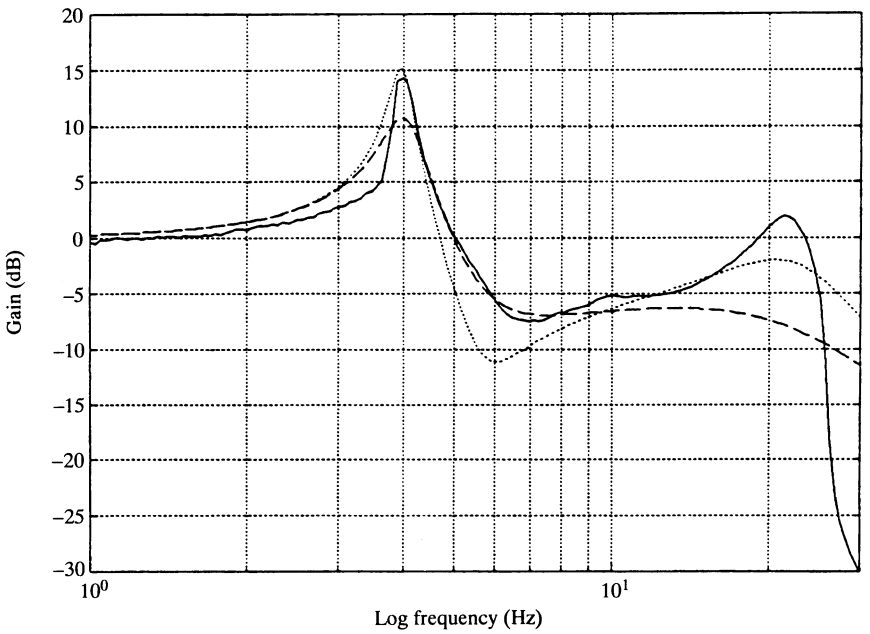

Fig. 4b Passive frequency response gain (unsprung mass acceleration/ground acceleration), experimental 2.5 mm input (solid line), theoretical $R = 1 \times 10^{10}$ (dashed line) and theoretical $R = 0.5 \times 10^{10}$ (dotted line)

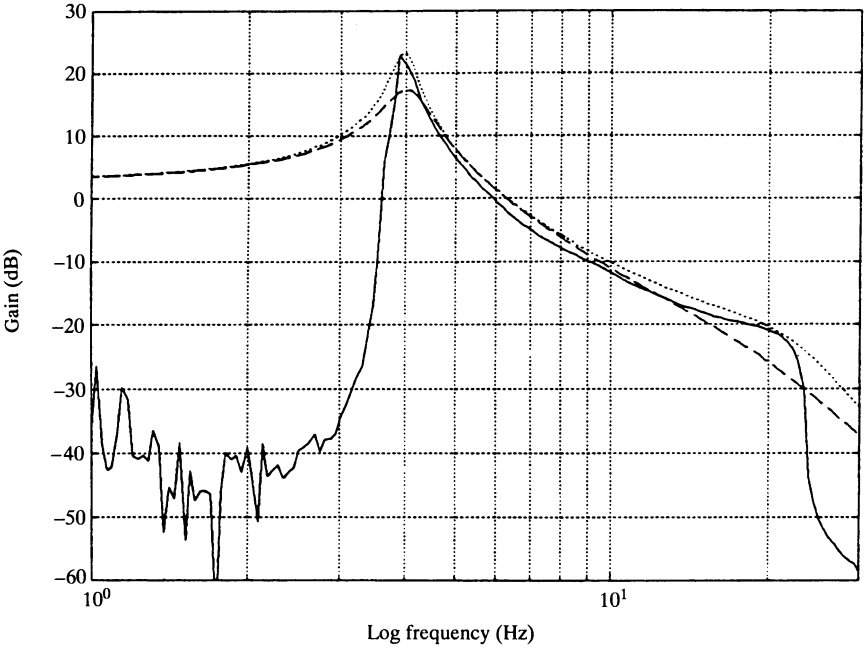

Fig. 4c Passive frequency response gain (ride height/ground acceleration), experimental 2.5 mm input (solid line), theoretical $R = 1 \times 10^{10}$ (dashed line) and theoretical $R = 0.5 \times 10^{10}$ (dotted line)

was calculated and a constant correction signal was applied for the next one second period. Thus, the suspension system was open-loop except when the corrective action was taken every second to prevent the actuator reaching the limits of its stroke. This technique proved very effective during this part of the testing and only with the largest input did the suspension come close to the limits of its travel.

The effects of increasing the amplitude of the input voltage on the ride height and body acceleration are shown in Fig. 5a and b. For both responses the effect of non-linear friction is seen again clearly on the 0.1 to 0.3 V [root mean square (r.m.s.)] input responses by the reduced resonant peak at 4 Hz. Once the input amplitude exceeds 0.4 V (r.m.s.) the gain at resonance remains constant, as would be expected. For an input amplitude of 0.5 V (r.m.s.) the open-loop responses for the ride height, body acceleration and unsprung mass acceleration are given in Fig. 6.

The open-loop response for the ride height, Fig. 6a, shows a resonance (complex conjugate pole pair) at approximately 4 Hz and an anti-resonance (complex conjugate minimum phase zero pair) at about 5.4 Hz. The zeros are a resonance of a constrained substructure (**11**) and in this case represent the body and unsprung mass

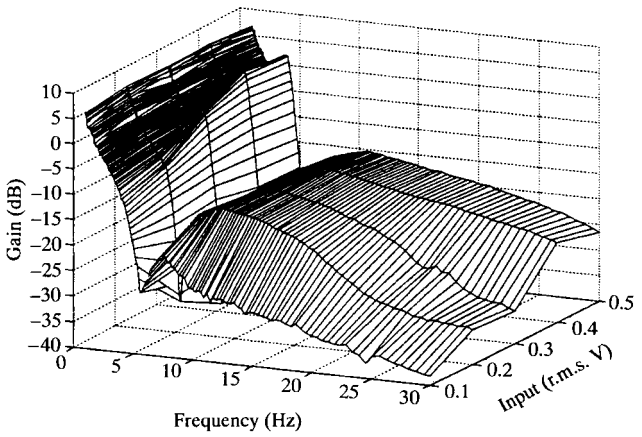

Fig. 5a Open-loop frequency response (ride height/input), three-dimensional frequency and input versus gain

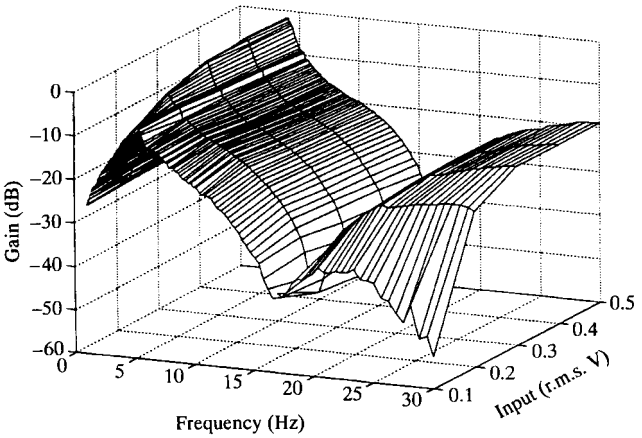

Fig. 5b Open-loop frequency response (body acceleration/input), three-dimensional frequency and input versus gain

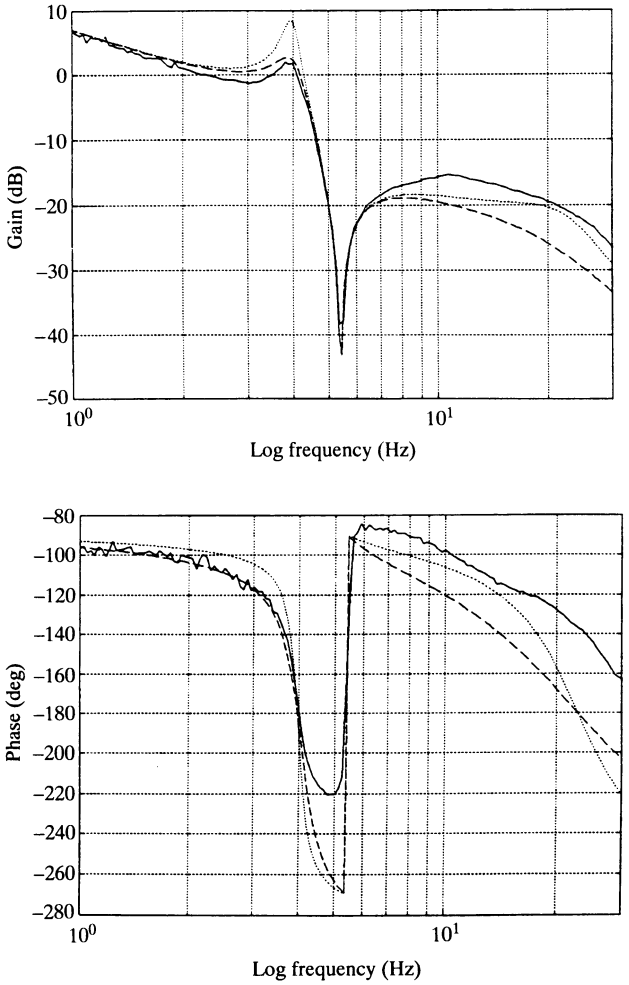

Fig. 6a Open-loop frequency response gain (ride height/input) (*top*), and open-loop frequency response phase (ride height/input) (*bottom*), experimental 0.5 V (r.m.s.) input (solid line), theoretical $R = 1 \times 10^{10}$ (dashed line) and theoretical $R = 0.5 \times 10^{10}$ (dotted line)

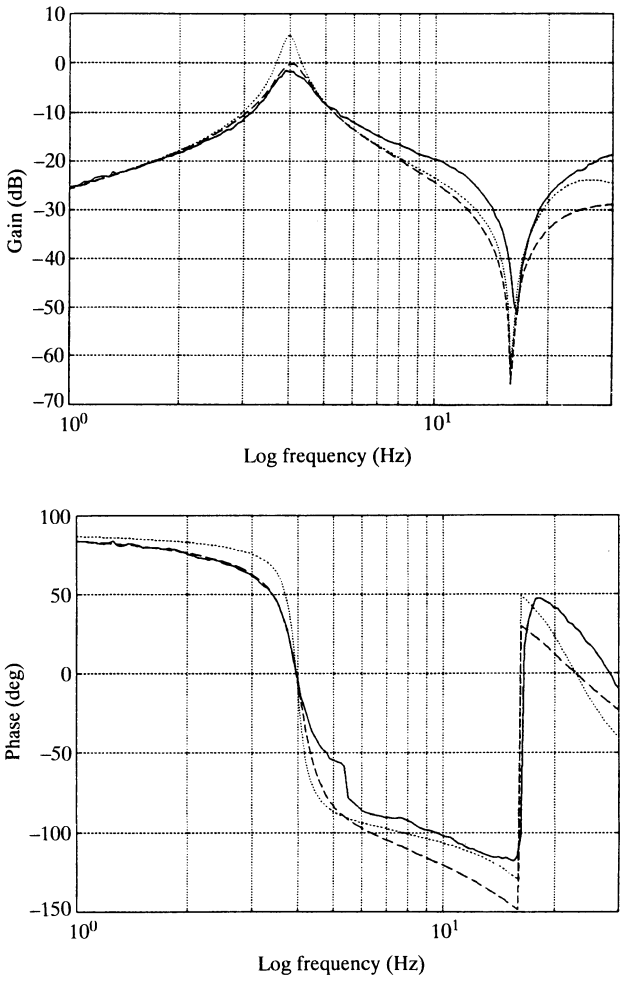

Fig. 6b Open-loop frequency response gain (body acceleration/input) (*top*) and open-loop frequency response phase (body acceleration/input) (*bottom*), experimental 0.5 V (r.m.s.) input (solid line), theoretical $R = 1 \times 10^{10}$ (dashed line) and theoretical $R = 0.5 \times 10^{10}$ (dotted line)

being locked together. The phase starts at 90°; this indicates the presence of a single integrator, which is borne out by the low-frequency slope of the gain relationship (−20 dB/decade). Thus the transfer function for this response will be type 1, see the Appendix. The maximum phase lag, between 1 and 30 Hz, is 220° and occurs at about 5 Hz. The anti-resonance occurs at the natural frequency of the total mass (body and unsprung) acting on the tyre; this is given by $\sqrt{[k_t/(m_s + m_u)]} = 33.9$ rad/s or 5.4 Hz, which is close to that measured experimentally.

The open-loop response for the body acceleration, Fig. 6b, shows a resonance at approximately 4 Hz and an anti-resonance at 16.6 Hz. The phase starts at +90° which indicates a single differentiator, this is also borne out by the low-frequency slope of the gain relationship. Thus, the transfer function for this response will be type −1, see the Appendix. The maximum phase lag, between 1 and 30 Hz, occurs at about 16 Hz and is approximately 120°. The anti-resonance occurs at the natural frequency of the unsprung mass acting on the tyre (body restrained) and is given by $\sqrt{(k_t/m_u)} = 100.7$ rad/s or 16.0 Hz, this is 0.6 Hz less than that measured experimentally and is probably caused by the level of passive damping in the system. Note that this is not the same as wheel hop. The open-loop responses for the unsprung mass acceleration are shown in Fig. 6c. These again show a resonance at 4 Hz and no zeros.

4.3 Closed-loop testing

The results from the passive and open-loop testing described above were used to select a suitable coefficient for the damper valve flow restrictor. This was essential for the controller design. A comparison between the experimental and theoretical responses is given below. The mathematical model developed was used to design a controller for the

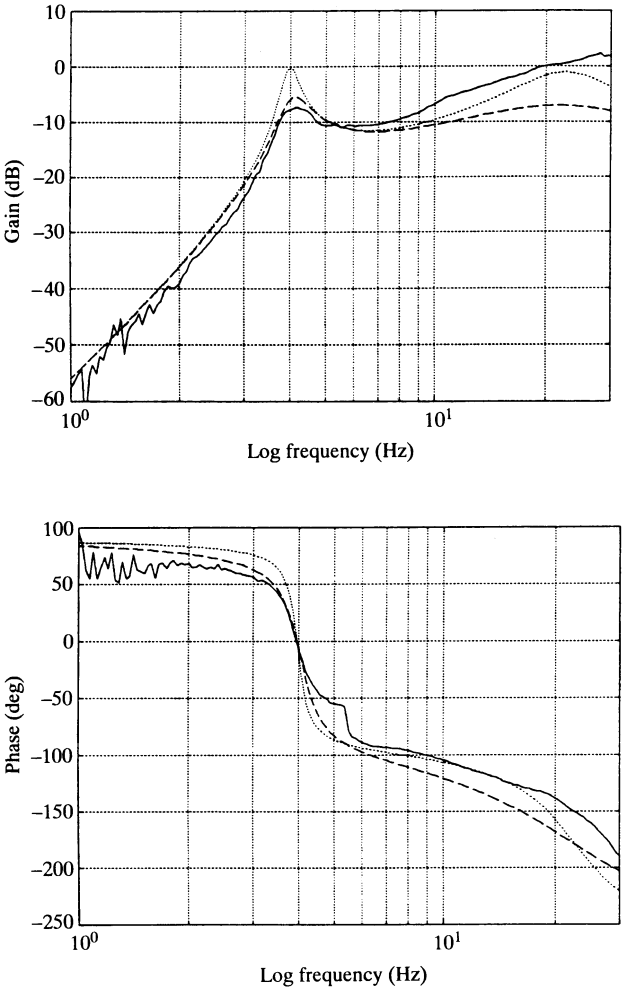

Fig. 6c Open-loop frequency response gain (unsprung mass acceleration/input) (*top*), and open-loop frequency response phase (unsprung mass acceleration/input) (*bottom*), experimental 0.5 V (r.m.s.) input (solid line), theoretical $R = 1 \times 10^{10}$ (dashed line), theoretical $R = 0.5 \times 10^{10}$ (dotted line)

active suspension system, which was tested on the quarter car suspension test facility.

5 THEORETICAL RESPONSES

The initial problem was to select an appropriate value of damper valve restrictor. This was done by fitting the theoretical responses to those from the experimental suspension system. Using this method, two possible values for the restrictor were obtained. One from the open-loop responses ($R \approx 1 \times 10^{10}$) and one from the passive responses ($R \approx 0.5 \times 10^{10}$). A comparison between the open-loop and passive experimental and theoretical responses for the two values of restrictor are shown in Figs 4 and 6. These show that for frequencies less than 10 Hz the open-loop responses are more accurately modelled by the higher level of damping, while the lower level of damping more accurately represents the passive responses. There is also an indication from the plots that the level of damping is frequency dependent and reduces at higher frequency. A parameter locus of the poles of the model for variations in restrictor value is shown in Fig. 7, with the two possibilities highlighted. This plot shows that the damper valve restrictor has greatest effect on the higher frequency (wheel hop) mode, while the lower frequency (body) mode reaches a maximum possible damping ratio of approximately 0.17. The increase in the effective damping of the open-loop responses is thought to be caused by the flow losses in the pipe between the servovalve and actuator.

The value of flow restriction measured in the open-loop tests was selected for use in the mathematical model, because the open-loop responses have a direct relationship to the stability when the system is run in closed loop. This is especially so at low frequencies, where the gain and phase crossover frequencies will occur. This results in a damping ratio of approximately 0.7 for the higher frequency (wheel hop) mode and 0.1 for the lower frequency (body) mode.

6 CONTROLLER DESIGN

The requirement was for a simple controller structure which allowed control over the primary functions of the suspension system. The three primary functions of the suspension in this situation are:

(a) to control the ride height;
(b) to minimize the tyre force variation;
(c) to improve the ride quality.

The classical structure often selected for an active suspension system (**4**–**7**) has ride height and absolute body velocity being fed back. It is also well established that in the design of a control system, acceleration feedback is also capable of enhancing the level of damping. An

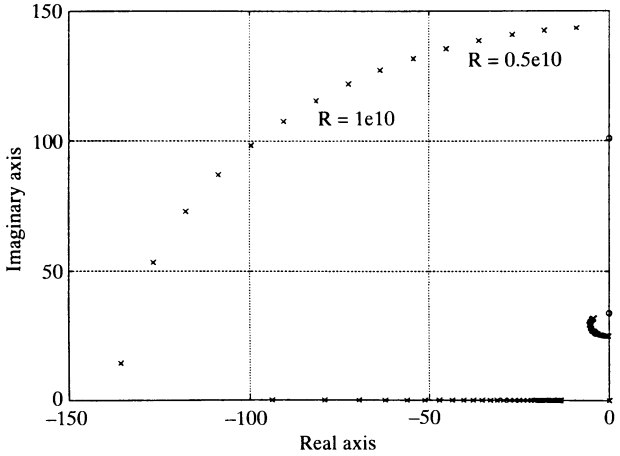

Fig. 7 Parameter locus plot for the suspension model for variations in the damper valve coefficient R from 0.1×10^{10} to 2×10^{10}

additional advantage is that it does not require an integration, with the stability problems caused by its associated 90° of phase lag.

For this active suspension system, the control loop shown in Fig. 8 was used. This is based on a cascade structure with an inner loop controlling body acceleration and an outer loop controlling the ride height. Both loops have a single proportional controller gain to be selected. There are two prime motivations for this structure:

1. The inner loop will help to reduce the effects of non-linear friction, which have been shown to affect both the open-loop and passive responses.
2. The interaction between the loops should be minimal because the inner loop (type 1) will have little effect at low frequencies, while the outer loop (type 1) will have its main effect at low frequency.

The controller was designed using the technique of sequential loop closure, starting with the inner loop. The parameters were chosen from root locus plots for variations in the appropriate controller gain. The value for the damper valve restrictor was selected from the open-loop testing.

Antialiasing filters were included to filter the sensor signals because the controller was implemented digitally; these were second-order Butterworth filters with break frequencies of 100 Hz. Though the controller was digital, it had been designed in the Laplace domain because the intended implementation frequency was over ten times the bandwidth of the suspension system (**12**).

6.1 Inner loop body acceleration

A root locus plot for variations in the inner loop controller gain K_a is shown in Fig. 9. Only the upper half of the complex plane is discussed because the lower half is a mirror image through the real axis. As the controller gain increases, the two loci A and B start to move away from the imaginary axis, before rotating clockwise and then moving back towards it. Locus A would, for infinite gain, finish on the zero shown. This condition, if possible, would indicate perfect body acceleration control with the unsprung mass acting on the tyre alone. A third locus C moves in towards the origin along the negative real axis.

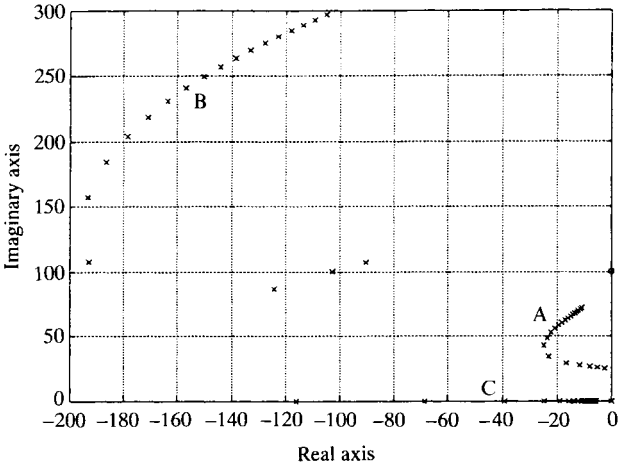

Fig. 9 Root locus plot for the inner loop with variations in the acceleration gain K_a from 0 to 20

From this root locus plot a value of $K_a = 4$ was selected. A normalized closed-loop frequency response of the inner loop is shown in Fig. 10; this shows that it has a bandwidth from 3 to 7 Hz.

6.2 Outer loop ride height

A root locus for variations in K_p is shown in Fig. 11. A damping ratio of approximately 0.7 was obtained for locus B for $K_p = 1.0$, while locus A has a damping ratio of less than 0.4. An open-loop frequency response for the outer

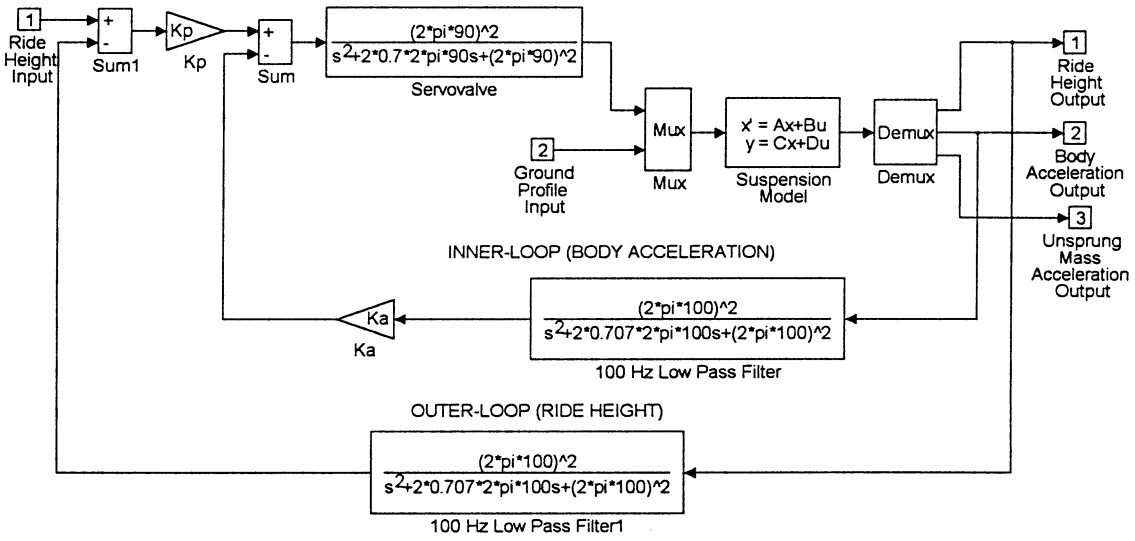

Fig. 8 Closed-loop active suspension control system

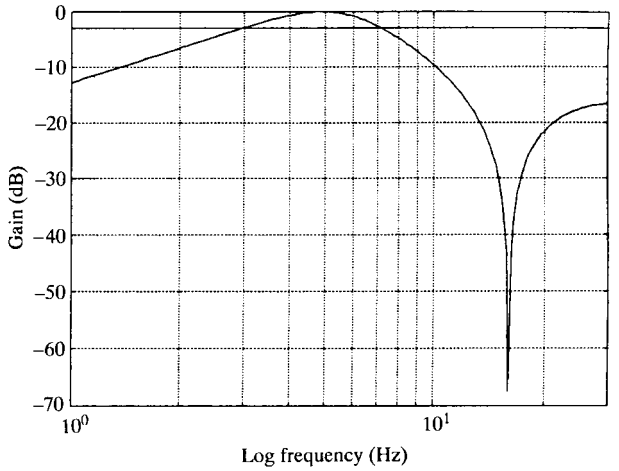

Fig. 10 Closed-loop frequency response of inner loop with peak normalized to 0 dB; solid horizontal line is at −3 dB

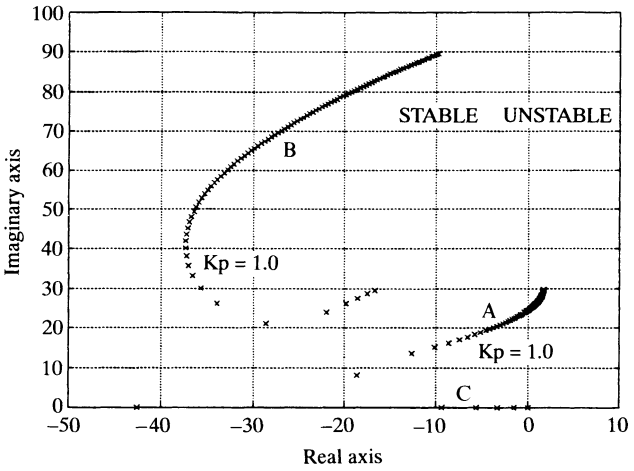

Fig. 11 Root locus plot for the outer loop with variations in gain K_p from 0 to 10 in steps of 0.1

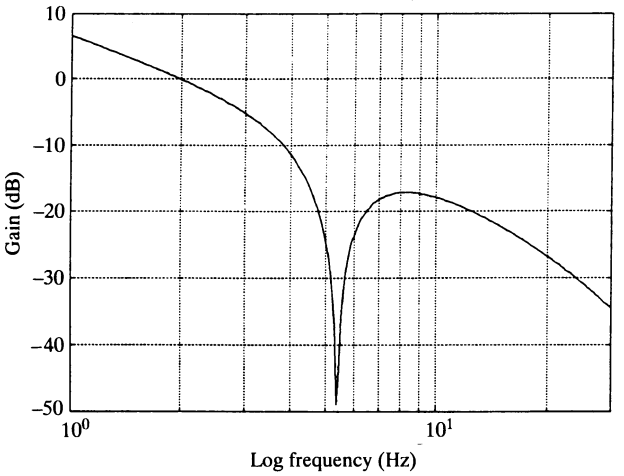

Fig. 12a Open-loop frequency response for the outer loop gain

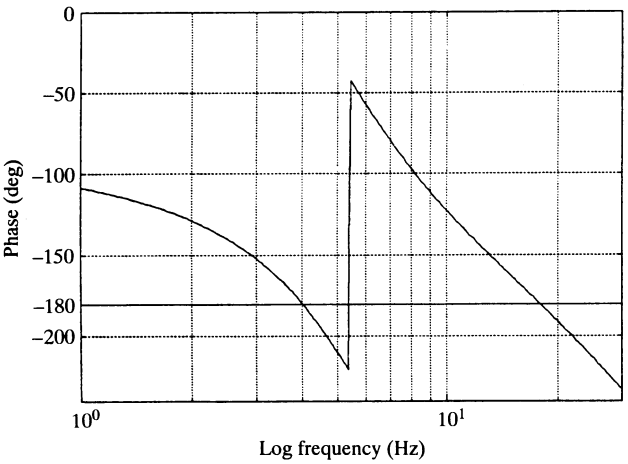

Fig. 12b Open-loop frequency response for the outer loop phase

loop, for $K_p = 1.0$, is shown in Fig. 12, from which the phase and gain margins are 60° and 12 dB.

7 CLOSED-LOOP SUSPENSION RESPONSES

The experimental suspension system was tested with the controller gains selected above ($K_p = 1.0$ and $K_a = 4.0$) and compared to those from the model. The active suspension controller was implemented digitally at 200 Hz.

An initial test was made to determine the response to a demand in ride height. The closed-loop response for a 0.5 V (r.m.s.) input, which represents a suspension displacement of 7.8 mm for a d.c. signal, is shown in Fig. 13a. There is close correlation between the theoretical and experimental results, with a bandwidth of approximately 3.5 Hz being indicated by both. This indicates good ride height control up to that frequency. The resonant amplitude for the theoretical results at 2.5 Hz is about 1 dB greater than that measured experimentally. It is thought that this is caused by the non-linear friction, which has not been incorporated into the model.

The response of the body to a 2.5 mm amplitude ground input is shown in Fig. 13b. The theoretical response has a higher gain than the experimental, below 16 Hz, indicating that the predicted response would be marginally worse than that measured. The resonant peak for the practical results has been reduced from 20 dB at 4 Hz for the passive suspension, to about 5 dB at 3 Hz for the active suspension.

The unsprung mass response to a ground input, Fig. 13c, shows good correlation up to 7 Hz. Above 7 Hz the theoretical results indicate a greater attenuation up to 22 Hz than occurs experimentally. The experimental results remain close to 0 dB up to 18 Hz; this would give less tyre force fluctuation than that predicted. This effect cannot yet be explained and is a characteristic of the experimental apparatus which will require further investigation.

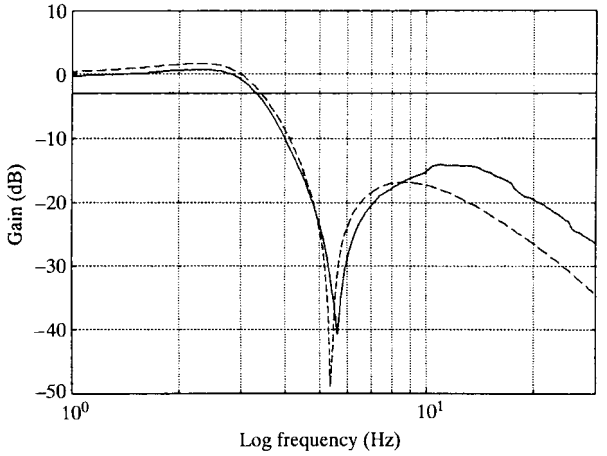

Fig. 13a Closed-loop frequency response outer loop gain, experimental 0.5 V (r.m.s.) input (solid line), theoretical (dashed line), solid horizontal line is at −3 dB

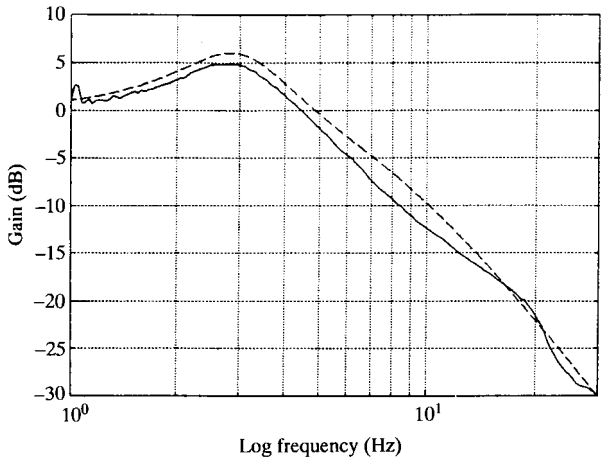

Fig. 13b Closed-loop frequency response gain (body acceleration/ground acceleration), experimental 2.5 mm input amplitude (solid line) and theoretical (dashed line)

Experimental plots of body acceleration and ride height against ground input amplitude are shown in Fig. 14. These show that the active suspension system is not as sensitive to non-linear friction as it was passively.

Plots comparing the experimental passive and active suspension results for the body and unsprung mass acceleration, and ride height to a 2.5 mm ground input, are shown in Fig. 15. Figure 15a therefore demonstrates an improvement in ride by reducing the peak acceleration by 15 dB and lowering its frequency by over 1 Hz. Figure 15b shows that in the active case there is little variation between the ground input and motion of the unsprung mass. This infers constant tyre displacement and hence reduced tyre force variation. This figure shows a reduction in both of the resonant peaks. Thus the aims of better control of the ride

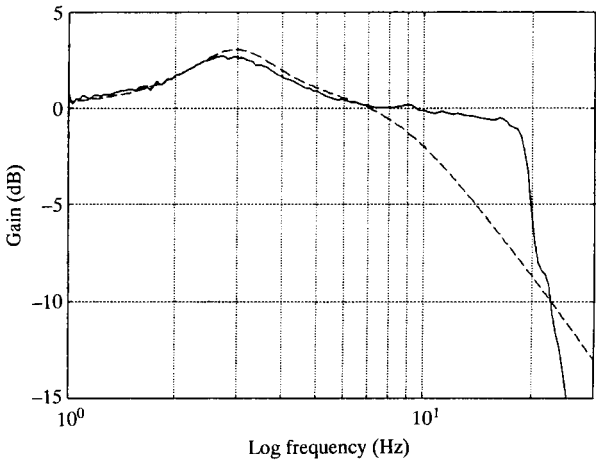

Fig. 13c Closed-loop suspension frequency response gain (unsprung mass acceleration/ground acceleration), experimental 2.5 mm input amplitude (solid line) and theoretical (dashed line)

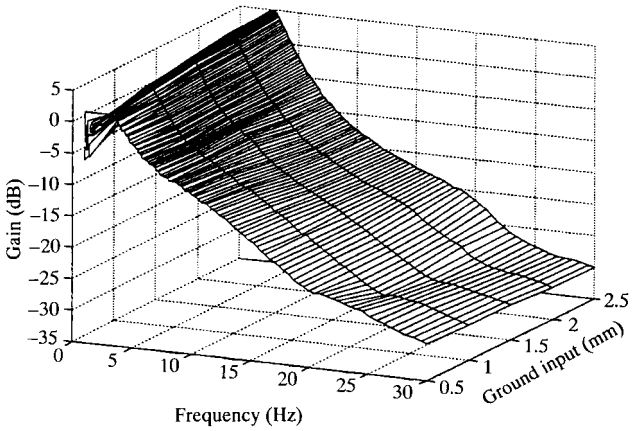

Fig. 14a Closed-loop frequency response (body acceleration/ground acceleration), three-dimensional frequency and ground input versus gain

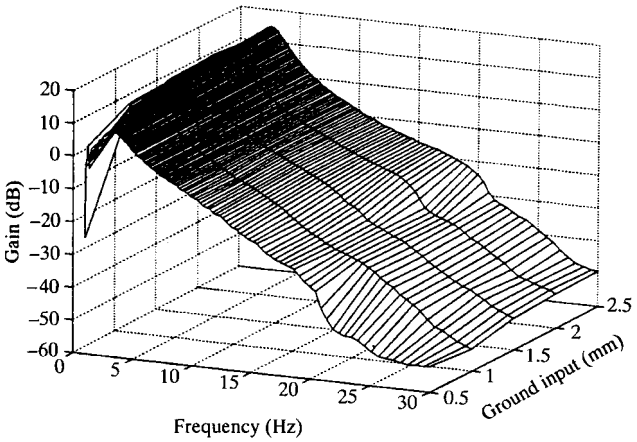

Fig. 14b Closed-loop frequency response (ride height/ground acceleration), three-dimensional frequency and ground input versus gain

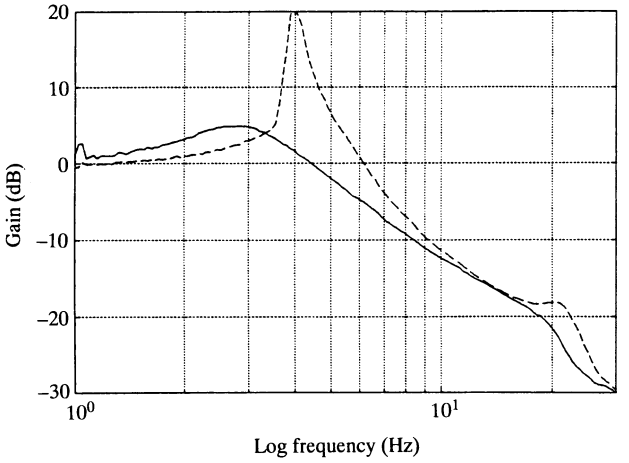

Fig. 15a Comparison between the experimental body acceleration/ground acceleration active (solid line) and passive (dashed line) suspension

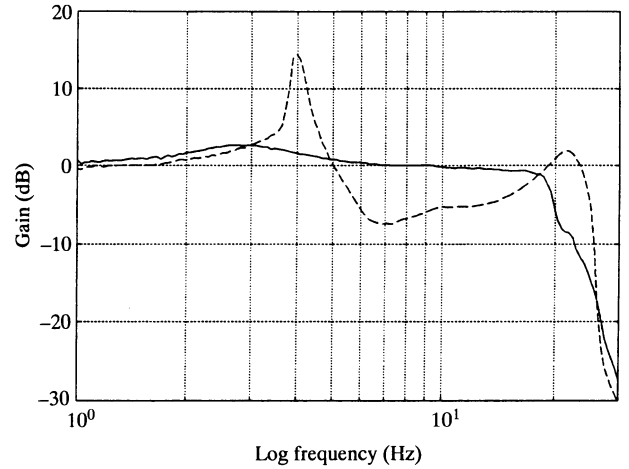

Fig. 15b Comparison between the experimental unsprung mass acceleration/ground acceleration active (solid line) and passive (dashed line) suspension

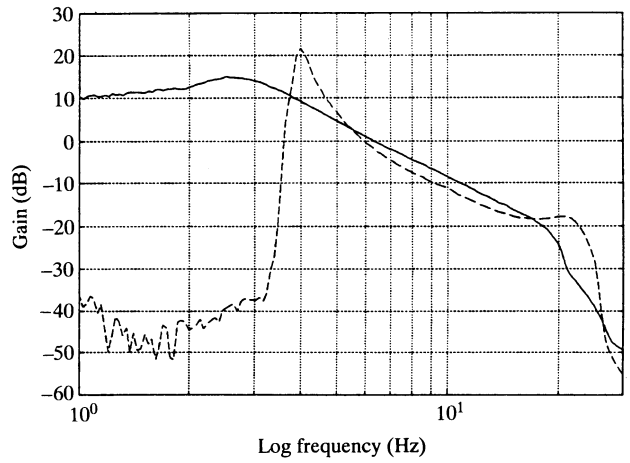

Fig. 15c Comparison between the experimental ride height/ground acceleration active (solid line) and passive (dashed line) suspension

height, reduced tyre force variation and improved ride quality have been achieved.

8 CONCLUSIONS

1. The design of an active suspension system for a racing car has been shown to improve the ride height control, to reduce tyre force variation and to improve the ride quality.
2. It has been shown that an experimental active suspension system can be adequately represented by a fifth-order linear model.
3. The effect of non-linear friction was shown to be greatest at low input levels. The suspension system appeared to have a reduction in damping as the frequency increased.
4. A simplified novel form of controller which was based on a cascade structure was used for the active suspension system. This consisted of an inner loop body acceleration controller and an outer loop ride height controller. This type of controller was selected because of its simplicity (only two gains for each wheel station) and its ability to reject the effects of non-linear friction.
5. The active suspension system designed was shown to give ride height control below 3.5 Hz, reduced tyre force variation and better ride quality than the passive system.
6. The controller designed was shown experimentally to give better results than those predicted theoretically.
7. It was demonstrated that a linear model can be used successfully to design an active suspension system, once an estimate to the level of low-frequency open-loop damping is determined.

REFERENCES

1 **Hac, A.** Adaptive control of vehicle suspension. *Vehicle System Dynamics*, 1987, **16**, 57–74.
2 **Kiriczi, S.** and **Kashani, R.** Robust control of active car suspension with model uncertainty using H_∞ methods. *Trans. ASME, Advanced Automotive Technologies*, 1991, **40**, 375–390.
3 **Wilson, D. A., Sharp, R. S.** and **Hassan, S. A.** The application of linear optimal control theory to the design of active automotive suspensions. *Vehicle System Dynamics*, 1986, **15**, 105–118.
4 **Cole, D. J.** Design, analysis and testing of a slow-active car suspension. Proceedings of IMechE International Conference on *Vehicle Ride and Handling*, November 1993.
5 **Elmadany, M. M.** Ride performance potential of active fast load leveling systems. *Vehicle System Dynamics*, 1990, **19**, 19–47.
6 **Karnopp, D.** Active damping in road vehicle suspension systems. *Vehicle System Dynamics*, 1983, **12**, 291–316.
7 **Truscott, A. J** and **Burton, A. W.** On the analysis, modelling and control of an advanced automotive suspension system. *CONTROL '94*, 21–24 March 1994, Conference Publication 389 (Institution of Electrical Engineers).
8 **Williams, R. A., Best, A.** and **Crawford, I. L.** Refined low frequency active suspension. Proceedings of IMechE Interna-

tional Conference on *Vehicle Ride and Handling*, November 1993.
9 MOOG E760 Servovalves data sheet (Moog Controls Limited, Ashchurch, Tewkesbury, Gloucestershire).
10 **Ljung, L.** *Systems Identification – Theory for the User*, 1987, pp. 365–369 (Prentice Hall).
11 **Miu, D. K.** Physical interpretation of transfer function zeros for simple control systems with mechanical flexibilities. *J. Dynamic Systems, Measurement and Control*, September 1991, **113**, 419–424.
12 **Franklin, G. F., Powell, J. D.** and **Workman, M. L.** *Digital Control of Dynamic Systems*, 2nd edition, 1990 (Addison Wesley).
13 **Franklin, G. F., Powell, J. D.** and **Emami-Naeini, A.** *Feedback Control of Dynamic Systems*, 2nd edition, 1991 (Addison Wesley).

APPENDIX

Theoretical quarter car suspension model in transfer function form

The quarter car suspension model can be developed in transfer function form by manipulating equations (1) to (5) or directly from the state space form equation (6) using (**13**)

$$\mathbf{H}(s) = \mathbf{C}(s\mathbf{I} - \mathbf{A})^{-1}\mathbf{B} + \mathbf{D} \tag{7}$$

Using either of the above methods the main transfer functions for the quarter car suspension model are

$$\frac{(X_s - X_u)}{Q_i}(s) = \frac{a_p k_d(k_t + (m_s + m_u)s^2)}{s(\alpha s^4 + \beta s^3 + \gamma s^2 + \delta s + \varepsilon)} \tag{8}$$

$$\frac{s^2 X_s}{Q_i}(s) = \frac{s a_p k_d(k_t + m_u s^2)}{(\alpha s^4 + \beta s^3 + \gamma s^2 + \delta s + \varepsilon)} \tag{9}$$

$$\frac{s^2 X_u}{Q_i}(s) = \frac{-s^3 a_p k_d m_s}{(\alpha s^4 + \beta s^3 + \gamma s^2 + \delta s + \varepsilon)} \tag{10}$$

$$\frac{(X_s - X_u)}{s^2 X_z}(s) = \frac{-a_d^2 k_t m_s}{(\alpha s^4 + \beta s^3 + \gamma s^2 + \delta s + \varepsilon)} \tag{11}$$

$$\frac{s^2 X_s}{s^2 X_z}(s) = \frac{a_p^2 k_t(k_d + a_d^2 R s)}{(\alpha s^4 + \beta s^3 + \gamma s^2 + \delta s + \varepsilon)} \tag{12}$$

$$\frac{s^2 X_u}{s^2 X_z}(s) = \frac{k_t(a_d^2 m_s s^2 + a_d^2 a_p^2 R s + a_p^2 k_d)}{(\alpha s^4 + \beta s^3 + \gamma s^2 + \delta s + \varepsilon)} \tag{13}$$

where

$$\alpha = a_d^2 m_s m_u$$

$$\beta = a_d^2 a_p^2 m_s R + a_d^2 a_p^2 m_u R$$

$$\gamma = (a_p^2 k_d + a_d^2 k_t) m_s + a_p^2 k_d m_u \tag{14}$$

$$\delta = a_d^2 a_p^2 k_t R$$

$$\varepsilon = a_p^2 k_d k_t$$

The location of the transfer function zeros which are not at the origin are shown in Table 2.

Table 2 Transfer function zeros not at the origin

Equation number	Zero(s) not at origin	Value
(8)	$\pm j\sqrt{\left(\frac{k_t}{m_s + m_u}\right)}$	$\pm j33.9$
(9)	$\pm j\sqrt{\left(\frac{k_t}{m_u}\right)}$	$\pm j100.7$
(12)	$-\frac{k_d}{a_d^2 R}$	-0.042
(13)	$\frac{-a_p^2 R + (a_p/a_d)\sqrt{(a_p^2 a_d^2 R^2 - 4 m_s k_d)}}{2 m_s}$	$-10.54 \pm j33.9$